Comparison of SPR and Edge Tracking as a Measure of Binding Kinetics in Whole Cells

By

Ashley Hunt

A Thesis Presented in Partial Fulfillment

of the Requirements for the Degree

Masters of Science

Approved October 2018 by the

Graduate Supervisory Committee:

Nongjian Tao, Chair

Chad Borges

Alexandra Ros

ARIZONA STATE UNIVERSITY

December 2018

ABSTRACT

Most drugs work by binding to receptors on the cell surface. These receptors can then carry the message into the cell and have a wide array of results. However, studying how fast the binding is can be difficult. Current methods involve extracting the receptor and labeling them, but both these steps have issues. Previous works found that binding on the cell surface is accompanied with a small change in cell size, generally an increase. They have also developed an algorithm that can track these small changes without a label using a simple bright field microscope. Here, this relationship is further explored by comparing edge tracking results to a more widely used method, surface plasmon resonance. The kinetic constants found from the two methods are in agreement. No corrections or manipulations were needed to create agreement. The Bland-Altman plots shows that the error between the two methods is about 0.009 s^{-1}. This is about the same error between cells, making it a non-dominant source of error.

TABLE OF CONTENTS

Page

LIST OF TABLES

Table Page

LIST OF FIGURES

Figure Page

Figure Page

Introduction

Receptor-ligand reactions are central to much of the field of biochemistry and pharmacology. Receptors are most often proteins embedded in the plasma membrane that extend into both sides of the membrane. A chemical messenger, often hormones, will bind to the extracellular portion of the receptor. The receptor will then undergo a conformation change that spans into the cytoplasmic portion of the receptor. In this way, the environment outside the cell can affect the environment inside the cell without relying on transporting anything across the membrane. Figure 1a shows how a major class of receptors, G protein coupled receptors, work. This process is one of the most important and widely used ways for the body to talk to itself and to transfer information from different tissues. Understandably, 40% of drugs on the market target receptors, shown in figure 1b[1].

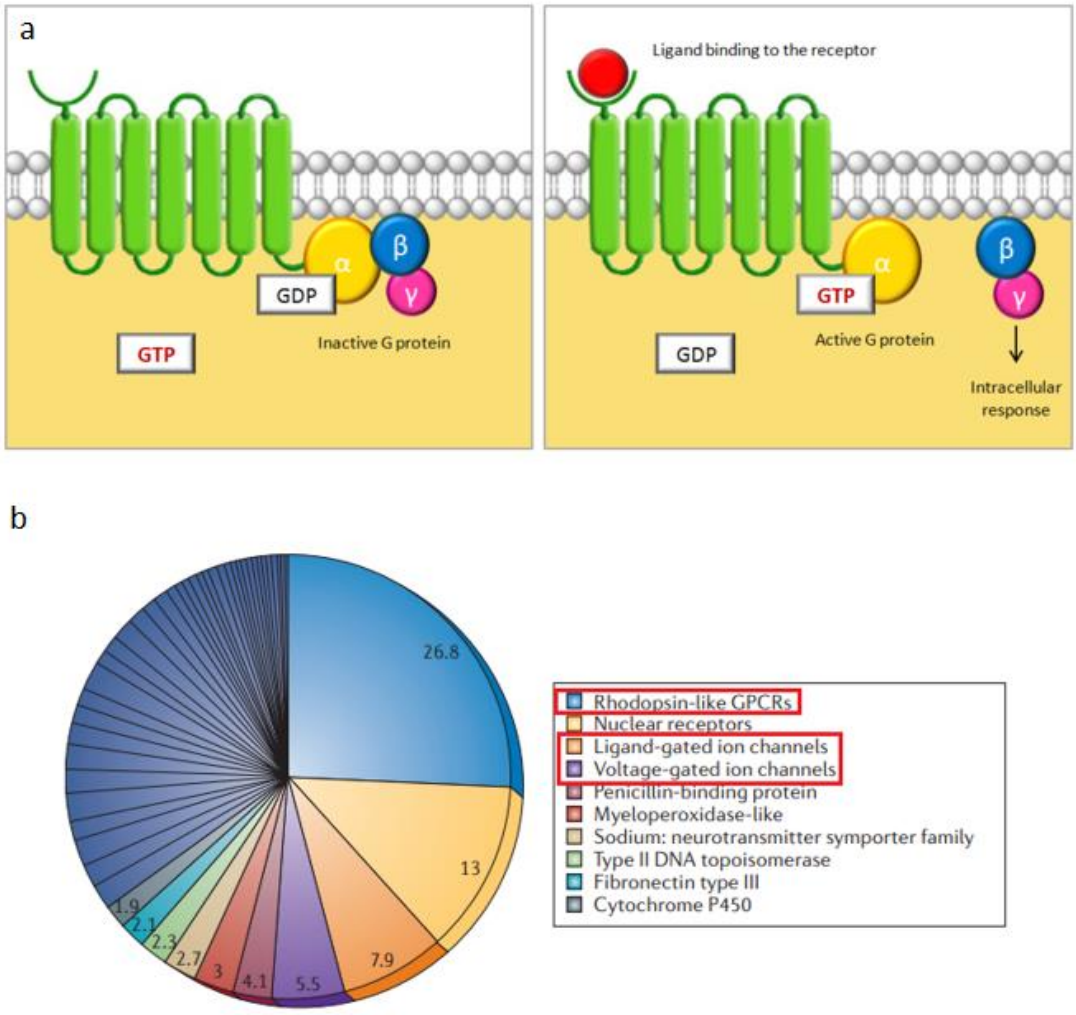

Figure 1 | Targets of the current FDA approved drugs on the market. a, the off (left) and on (right) states of a generic GPCR, showing how receptors function to carry messages across membranes. Figure taken from Alberts (2002)[2]. b, a pie chart of the FDA approved drugs on the market. Highlighted are three classes of membrane receptors, with GPCR being by far the most common. Figure from Overington (2016)[1].

Yet, for many of these reactions there is a lack of tools to characterize them. For receptor-ligand binding the equilibrium constant and the rate constant are two commonly used measures to understand a reaction. Together they describe how much of a ligand will bind and how fast it will bind. Just one alone provides an incomplete picture. This is

particularly true inside the blood stream, where most drugs act. Concentrations can change fast and often equilibrium is never reached, for example the commonly used drug glyceryl trinitrate only has a half-life of 3 minutes in blood[3]. In these cases the kinetic constants, which measure how fast the binding even will occur, can define the extent of binding. Since receptors usually stay in their 'on' conformation for as long as the ligand is bound, the kinetic constant of the dissociation is also very relevant.

There are several major challenges when studying receptor kinetics. Receptors are proteins embedded in the hydrophobic cell membrane with hydrophilic portions sticking out into the aqueous environment on both sides of the membrane. This amphiphilic nature introduces several issues with extraction and isolation. Extraction becomes a tedious, laborious task of physically separating the receptor from its membrane environment[4]. Detergents need to be added to keep the receptor stable and in solution with the ideal detergent mix varying greatly between receptors. There is also the ever lingering concern that the conformation of the receptor will change due to the detergents[5]. Some researchers have developed methods to move the receptors to vesicles to recreate its native environment; However, even this method may be lacking. The plasma membrane is a complex mixture of various lipids and proteins that is connected to a complex cytoskeleton, and vesicles can lack the properties that allow receptors to function the way they do in their native environment[6]. These issues plague the study of membrane receptors outside the membrane. Others have turned their focus to studying receptors inside whole cells, though the tools for this area are still being developed[7].

There are also difficulties more inherent to the field of chemistry, primarily in finding a way to monitor the reaction. Fluorescence labeling is commonly used but is not feasible for small molecules, since dyes are large molecules and can drastically change the properties of the species being studied. This poses a problem particularly to pharmacology since 89% of drugs are small molecules[1]. Radiolabeling is a sure way to not affect the binding or kinetics even with small molecules, but it carries major drawbacks: it is extremely costly, it brings the hazards of radioactive materials, and it demands custom synthesize of reagents.

The type of labeling also dictates if continuous monitoring is possible. Many labeling techniques, including radiolabeling and most types of fluoresce labeling, do not alter their signal if the receptor is bound or not. As a result of this, the reaction must be stopped, and the bound and unbound species separated before measurements can be taken. This would then only produce a single data point on a kinetics curve and would need to be repeated many times to just get one curve. This becomes infeasible with fast reactions that demand high time resolution. There are some methods, such as those that use FRET and chemiluminescence, that can achieve continuous monitoring, but require a carefully designed reaction scheme.

There are already a few platforms that side-step these issues. Surface plasmon resonance (SPR) and quartz crystal microbalance methods provide label-free and continuous monitoring. They work by immobilizing one reactant and placing it inside a microfluidics system to flow the other reactant over it. Binding is recorded by some change the physical properties of the surface in response to the addition of a bound

reactant, with both methods being mass dependent. Unfortunately, these methods often still require the extraction of receptors. While SPR is sometimes used with whole cells, it's incapable of detecting binding events higher than 100 nm above the surface.

The aim of this work is to develop a method that provides continuous label free monitoring and does not require extraction. This would be a method that avoids the largest pitfalls of the field and give a viable way to measure receptor-ligand binding kinetics. Extraction is avoided by working with whole cells. While other methods detect changes in physical properties of the surface the reaction is happening on, this method detects changes in the morphology of the cell that the reaction is happening on. It has been observed that the cell subtly changes in shape with binding. When a receptor is bound, it changes conformation to carry the message across the member. This changes how it rests in the plasma membrane, and as a result how the lipids wrap around the receptor, as shown in figure 2. When tens of thousands of these receptors undergo these changes, the overall shape of the plasma membrane changes as well.

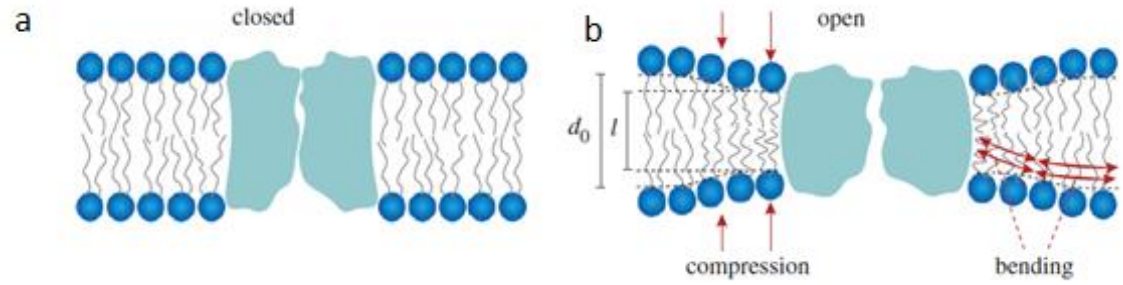

Figure 2 | How change in receptor confirmation affects surrounding lipids. a, an ion channel receptor in it's resting, closed state. The surrounding lipids are in a low energy state while they cover the hydrophobic portion of the receptor. b, the came receptor in an open state. It change shape to carry the message, in this case by opening a pore inside it. This change in shape changes how the hydrophobic and hydrophilic portion rest in the membrane. The lipids around it also deform in order to cover the hydrophobic section while still keeping the hydrophilic section exposed. This changes many mechanical properties of the membrane, which ultimately lead to a change in size. Figure from Lundbæk (2010)[8].

The changes are just 10-100 nm, but an algorithm developed to track edge movement can monitor these changes with just a typical light microscope and a 10X objective. A similar fluidics system typical to surface plasma resonance is used, where the cells are immobilized and a solution with the ligand flows over them. Combining these methods, a means to monitor the kinetics of ligand-receptor binding was developed while avoiding many issues that the field currently suffers from. Here the binding curves from the edge tracking method are compared to the binding curves obtained from a more established method: SPR. For this work, wheat germ agglutinin (WGA) was used as the ligand. WGA binds to the sugar N-acetyl-D-glucosamine which is attached to glycoproteins on the cell surface. It's attached to many different lipids and proteins on the

membrane and in different locations in sugar structures. The binding kinetics of WGA to N-acetyl-D-glucosamine was previous found to be $1.6 \cdot 10^{-7}$ M^{-1} when tested on whole cells[9]. Its large size makes it easily detectable in SPR, and it also causes large membrane deformation making it a good candidate to compare both methods.

Methods and Materials

Cell culture methods

Experiments used the SH-EP α4β2 cell line. All cell culturing protocols were done inside a biological safety cabinet (BSC). This is a neuroblastoma cell line derived from the SK-N-SH cell line. It was grown in DMEM (Lonza, 12-741F) supplemented with 10% FBS (Gibco, A31606-01) and 40 units/mL penicillin and 40 μg/ml streptomycin sulphate (Gibco, 10378-016) in 25 cm^2 flasks (Corning Falcon, 353108). Cells were passaged every 2 to 3 days, whenever 80% confluency was reached. Cells were briefly washed when passaging with 5 ml Hank's Buffered Salt Solution (Gibco, 14025-092). Then 2 ml of 0.05% trypsin-EDTA (Gibco 25200-056) was added and the flask was incubated at 37° C for approximately 1 minute, until the cells started to detach. The flask was then returned to the BSC and was rinsed with 3 ml of medium. The solution was then centrifuged at 900 RPM for 5 minutes, causing a pellet to form. The liquid was removed and the cells were suspended in 1 mL of medium, giving a concentration of roughly 10^5 cells per mL. A passage ratio of 1:5 or 1:7 was used to seed a new flask.

Chip preparation

22 mm by 22 mm gold coated cover slips were used. They were rinsed with ethanol followed by water before being blow dried with compressed nitrogen gas. Silicon wells with a volume of 800 uL were cleaned in the same way before being pressed onto the gold chips. Chips with wells were exposed to UV light for 5 minutes while in a sterile BSC. Type IV collagen (Sigma Aldrich, C5533-5MG) diluted to 10 ug/ml in PBS (Corning Cellgro, 21-040-CV) before being added to the wells. The wells contained 700 uL of collagen solution when incubated at 37° C and 100% RH for 2 hours. The collagen solution was then vacuumed out and the chips washed with HBSS.

Cells were passaged as described above. Some of the suspended cell solution was added to more medium to dilute it 100X. This diluted suspension was added to the collagen-modified chips. They were then placed back in a cell incubator. Incubation lasted only 1 hour, as which point the medium was vacuumed out and the cells were briefly washed with HBSS. Then room temperature 4% formaldehyde in PBS (Santa Cruz Biotechnology, SC-281692) was added for ten minutes. After ten minutes the formaldehyde was vacuumed out, and the cells washed with PBS three times. A final 700 uL of PBS was added and the cells were stored at 4° C until use. All cells were used within one day of being prepared.

Experimental protocol

Cells prepared as described above were monitored with a SPR based instrument from the company Biosening Instrument, the SPRm 200. This is a duel SPR-bright field instrument with a microfluidics and auto-sampler system; a schematic of the instrument is

shown in figure 3. The running buffer was 1X PBS at 250 uL per minute. Kinetics experiments involved a short, initial baseline reading followed by 2 minutes of exposure. After the exposure phase the solution returned to 1X PBS and the dissociation phase was recorded. The length of the time recorded varied between 2 and 5 minutes. All data was recorded at 1 fps. Blanks were drawn from a vial that contained 1X PBS. Calibration runs for the SPR videos used 0.9X PBS. Other leveled of diluted PBS were used to measure the response to osmotic pressures. Five different concentrations ranging from 5 to 100 ug/ml of the ligand wheat germ agglutinin (Sigma Aldrich, L9640-25MG) was used to study binding kinetics.

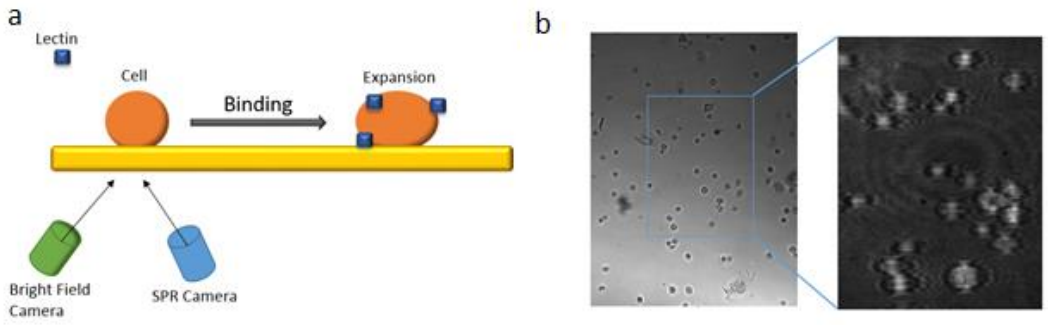

Figure 3 | Overview of how the SPRm 200 works. a, schematic showing the setup used. Cells are grown attached to gold chips and placed in a fluidics device where it is recorded by two cameras. One camera is set up to record SPR images and the other records bright field. As a ligand (in this case lectins) are introduced by the flow system expansion occurs. This edge expansion is measured and can be compared to SPR signals collected simultaneously. b, real images taken from the duel measurement instrument. The SPR camera captures only a quarter of the bright field area but provides greater pixel resolution.

For higher resolution, a cell trapping setup was used. This setup does not allow for SPR monitoring, but does give a significantly higher resolution with edge tracking. For these experiments, cells are fixed in suspension. The cell suspension in medium that

is used to seed a new flask is centrifuged for 5 minutes at 900 rpms. A pellet forms and the liquid is vacuumed out. The pellet is then suspended in 1 ml of room temperature 4% formaldehyde in PBS. It is incubated for 5 minutes, followed by 5 minutes of centrifugation at 900 rpm. Another pellet of fixed cells forms and the liquid is vacuumed out. The cells are again suspended in PBS and stored in 4° C until used.

EMD Millipore's specialized chip, the 150 μm AXIS™ Axon Isolation Device (shown in figure 4), was used for cell trapping. This chip was designed to grow neurons and to be able to separate the axons from the body. It is composed of a glass chip with PDMS attached to it. The PDMS has 4 open wells which were modified to have tubing attached. Each well is attached to another well with and channel that cells can move freely through. The two channels run parallel and are connected with roughly 100 microgrooves. These microgrooves are 10 μm wide and allow for solution to move through them, but not the cells. By applying a pressure gradient across the channels with simple syringes, cells in solution can be trapped. This setup allows for 40X phase contrast with clearer edges and larger displacements.

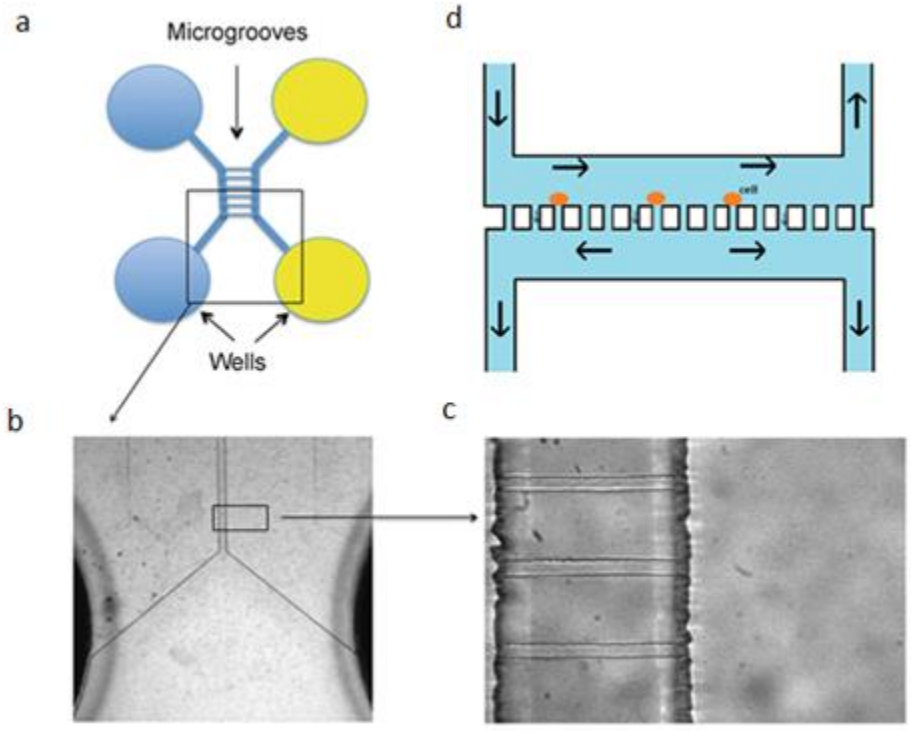

Figure 4 | Overview of the cell trapping setup. a, cartoon of how the cell trapping device looks to the naked eye This highlights the four wells, and that each pair is connected with a channel. The two channels are also connected with roughly a hundred microgrooves. b, a real image showing the channels attached to the wells (black areas). The two channels run parallel with a 150 μm gap between them. c, a real image of the gap between the two channels showing the 10 μm wide microgrooves. d, cartoon schematic of how the cell trapping device works. The orange ovals represent cells, and the arrows show the flow due to pressure gradients. A normal flow is run through one channel, where the cells are trapped. Syringes are used to give suction to the other channel. Flow moves through the microgrooves, with cells getting pulled towards them until they are trapped.

The last set of experiments involved polystyrene micro beads, with an average diameter of 10 μm. In order to aid with adhesion, polystyrene dissolved in acetone was pipetted onto a 22 mm by 22 mm coverslip. Once the acetone evaporated, a thin film of

polystyrene was left. A solution of polystyrene beads in water was placed on the modified chips and the chips incubated at 60° C overnight. This caused the beads to attach to the glass slide while still largely keeping their shape. A silicone well was placed on the chip and filled with PBS. The attached beads were monitored with a 40X, phase contrast miscopy with no flow.

Data Processing

SPR curves were extracted from videos using ImageJ. For calibration the background intensity on the 0.9X PBS runs were monitored. The intensity change between 1X PBS and 0.9X PBS was set to 23 mDeg, and this conversion factor was used for all further runs of the day set of videos. A new calibration curve was used for every new chip. Kinetic curves for WGA binding with glycoproteins were found by analyzing the cell edge in ImageJ. A region was selected along the cell edge and the average intensity change for the region was converted to mDeg and used as a kinetics curve.

The bright field data was processed with an algorithm developed in house, the steps of which are shown in figure 5. Once a differential intensity plot is made (figure 5F), it picks a location based on two criteria; if it is linear and how steep the slope is. This serves two purposes. This new location has the highest change in intensity, meaning any changes in cell size have the highest sensitivity there. Secondly, because it is linear, changes can be modeled linearly. The field of view in terms of micrometers is known and used to create a conversion factor between pixels and nanometers. The slope at the chosen point is then used to relate pixel movement with intensity changes, allowing us to relate intensity changes with distances in nanometers. Finally, the location of the adjacent

boxes is kept constant, and the differential intensity is recorded for every frame and converted to nanometers using the previous conversion factor.

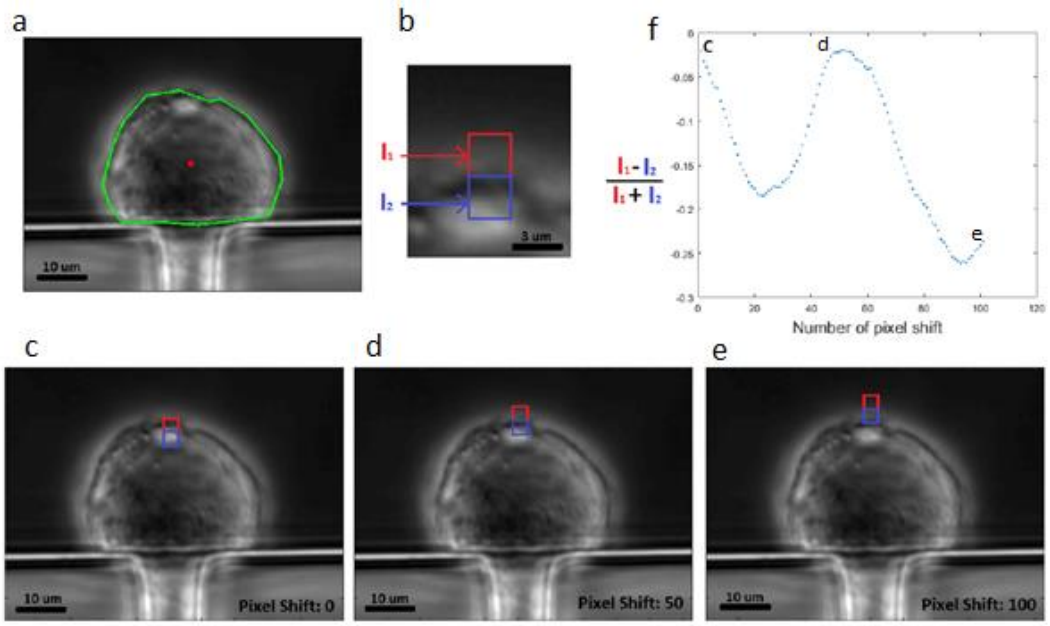

Figure 5 | Steps used in the algorithm to define the edge and relationship between intensity change and distance. A, the cell is manually outlined and the center is found based on the outline. B, two adjacent regions of interest are drawn on either side of the edge. The total intensity of each box is found and recorded. C-E shows the range of locations the ROIs are drawn on. While only three locations are shown, a total of a 100 pairs are drawn within this range. F, the differential intensity is found and plotted on the horizontal axis. The vertical axis records the pixels shifted. Based on this graph a location to record the intensities is decided, and the change in differential intensity with respect to displacement is noted.

Using this method, a displacement value relative to the first frame can be calculated for every frame. If the expansion is related to the number of bound receptor, one can get a kinetics curves.

Chapter 1: Osmotic pressures

One way to easily and reliably induce size changes is with osmotic pressures. The cell membrane does not permit ions to pass through, and the cytoplasm has a specific salt

concentration. When the cell is placed in a low salt solution, osmotic pressure across the membrane causes expansion. Conversely, a high salt solution causes contraction. The change should be linear with respect to salt concentration provided the strain is small enough[10]. While these tests are generally done with synthetic materials, the principles should hold true for plasma membranes. How large depends on the properties of the cell. The elasticity of the plasma membrane, and how that can vary with environments, has been studied for decades. The driving force behind this research is to understand how cells use the elasticity and tension of their membrane to do a wide range of functions. This includes the sensation of touch[11], motility[12], and moving proteins[13]. Various methods to probe the membrane have been used, but all have their limitations. Aspiration, optical tweezers, and atomic force microscopy are the most common methods to measure membrane tension[14]. The basic principles are shown in figure 6.

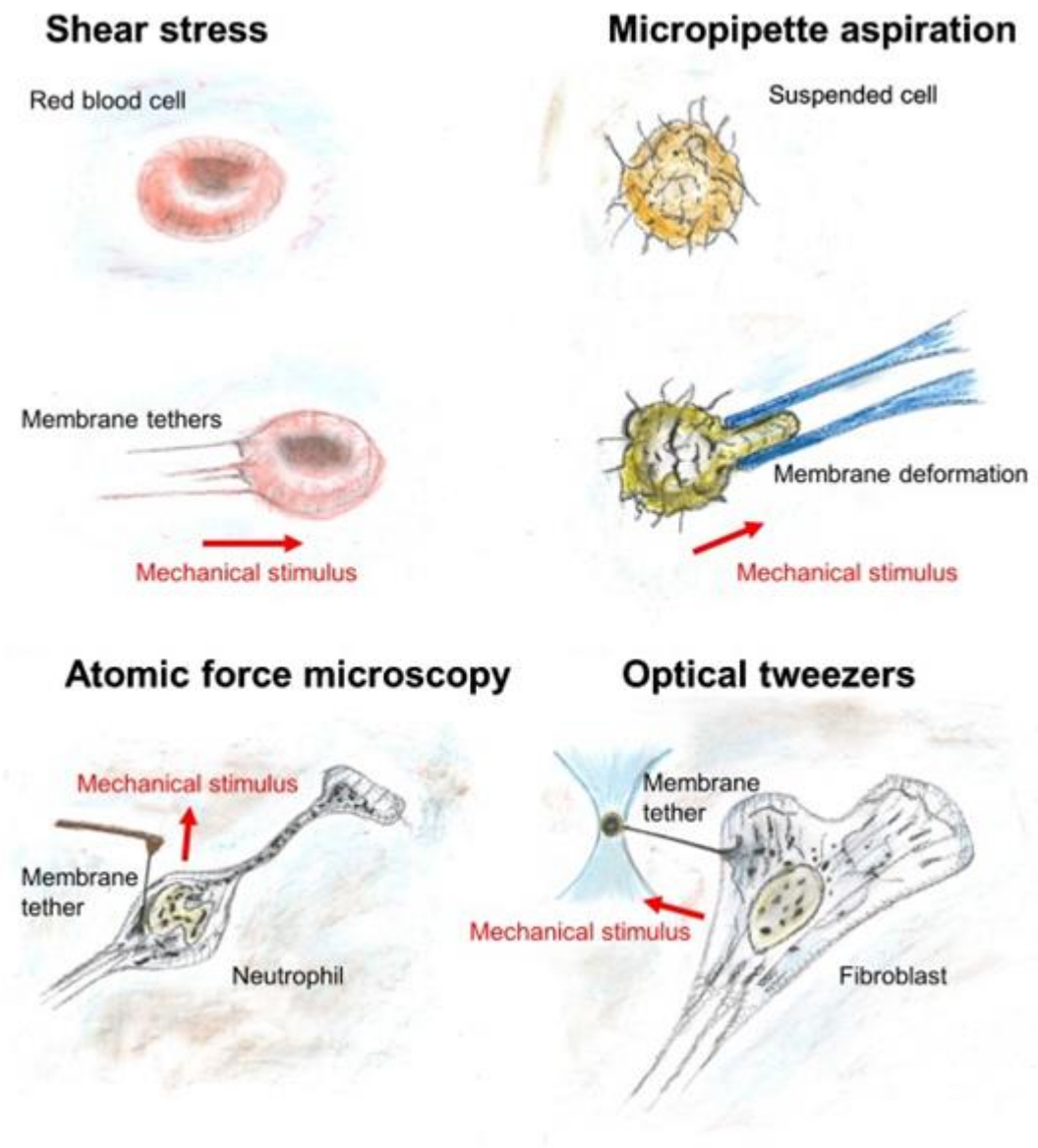

Figure 6 | Current methods used to test membrane tension. Most commonly, membrane tethers are used. These thin stretches of membrane are well studies and understood, but give limited results. Only one, small section of the membrane can be tested at a time. This gives localized results that may not be true for the whole cell. It also requires a lot of work to integrate something into the plasma membrane to allow for the creation of the tether. Figure from Pontes (2017)[14].

Each of the methods in figure 6 is limited to either suspended cells or adherent cells and cannot be used for both. Micropipette aspiration is the most commonly used

type for suspended cells, while singular membrane tethers are more exclusive for adherent cells. These methods tend to measure localized tension, and not tension of the whole cell. The different methods for different cell types makes comparison difficult between methods or cell types. The edge tracking algorithm has been shown to work for both cell types. Osmotic forces have been used to characterize the plasma membrane, but spatial and temporal resolution has been a hindrance[15]. The edge tracking algorithm can measure both adherent and suspended cells, and provide high resolution. It can also measure local changes all across the cell, giving both local and total measurements.

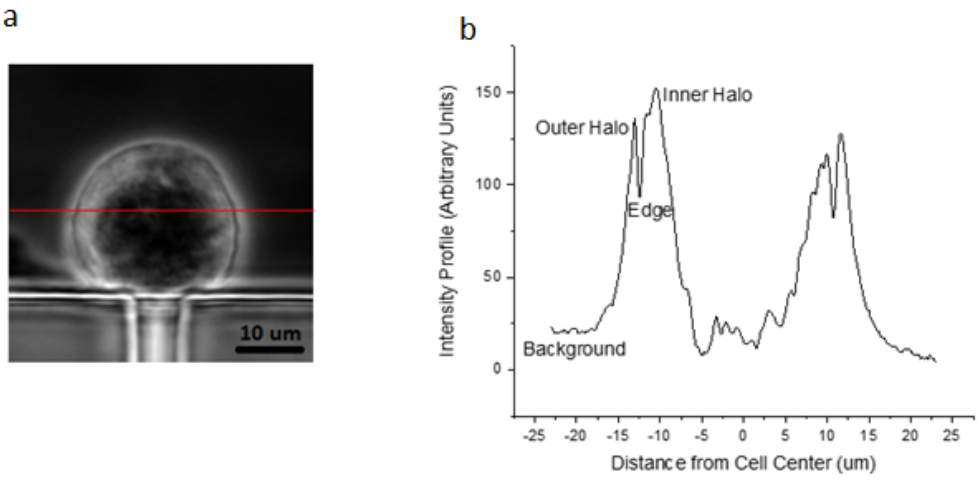

Figure 7 | Image from the cell trapping setup and its intensity profile. a, typical image of a trapped cell. The red line shows the trace used for part b. b, the intensity of each pixel along the red line. This shows a distinct pattern of the inner and outer halo, and the dark edge that separates them.

For these experiments, a cell trapping setup was used as described in the methods. Figure 7 shows a typical trapped cell inside a fluidics device. Though only one cell is shown, two cells can be measured at a time. This set uses a higher objective and uses phase contrast. The higher objective decreases the field of view and gives more pixels per

area. This is very useful when trying to measure such small changes, as each pixel is subjective to light noise. The phase contrast gives better contrast, particularly a dark background, bright halo, dark edge, and another increase in light immediately inside the cell. This distinctive and high contrast pattern gives a higher intensity differential, which the algorithm uses to calculate displacement.

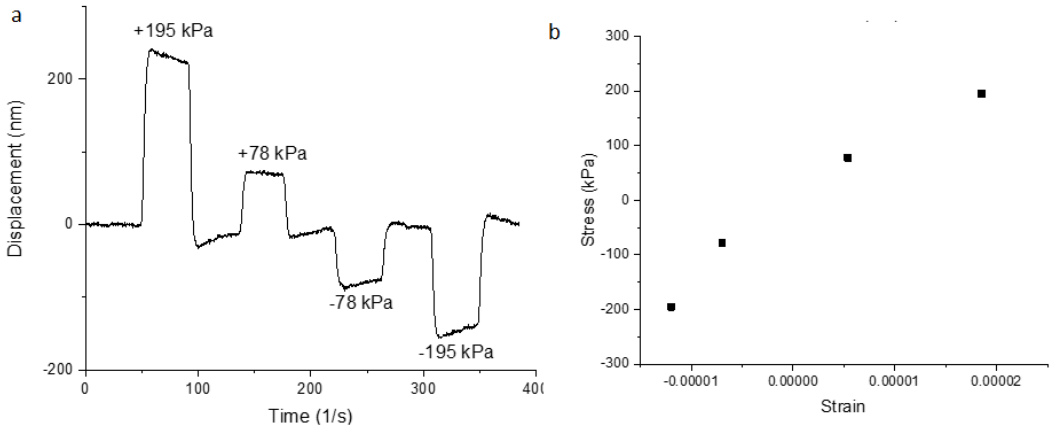

Figure 8 | Size changes from osmotic forces and the results stress-strain curve. a, the displacement of a single, trapped cell over the course of a few minutes. Different concentrations of PBS were introduced when indicated, and their resulting expansion was indicated. A negative expansion means contraction, which is expected with concentrated PBS due to higher salt concentrations. The initial PBS concentration was 1X, and in between the other concentration, it was returned to 1X. b, the stress-strain curve from part a. It appears to be linear with an R^2 value of over 0.95. However, because the inside of the membrane has a complex network of proteins, the cytoskeleton, it's not fair to assume to the moduli of expansion and contraction are the same.

Figure 8A shows the edge tracking as hypotonic and hypertonic solutions are added. Between each run 1X PBS was introduced and the membrane was allowed to relax back its resting state. Transitions between states were brief, and lasted just a few seconds. The stress was calculated using van't Hoff's equation relating osmotic pressure with osmolarity. The osmolarity was simply the differences in electrolyte concentration

inside and outside the cell. The unitless strain is the percent change in size, based on initial cell radius and measured displacement. In this figure, positive pressure is from a hypotonic solution, and negative pressures are from a high salt solution. This gives the stress-strain curves a positive slope. Figure 8B is the resulting stress-strain curve from figure 8A. The relationship seems linear, though this might not be the case. The cytoskeleton is a complex network of proteins that give the cell its structure and shape. How these proteins stretch is likely very different than how they compress. Since they contribute so much of structure of the cell, the difference in how they stretch and compress can change the overall mechanics of the cell. Figure 8B shows that there might be a change in slope across the origin, but more data points would be needed. Even if there is a change in slope, the change would be relatively small. This make sense biologically, since cells need to withstand both positive and negative pressures.

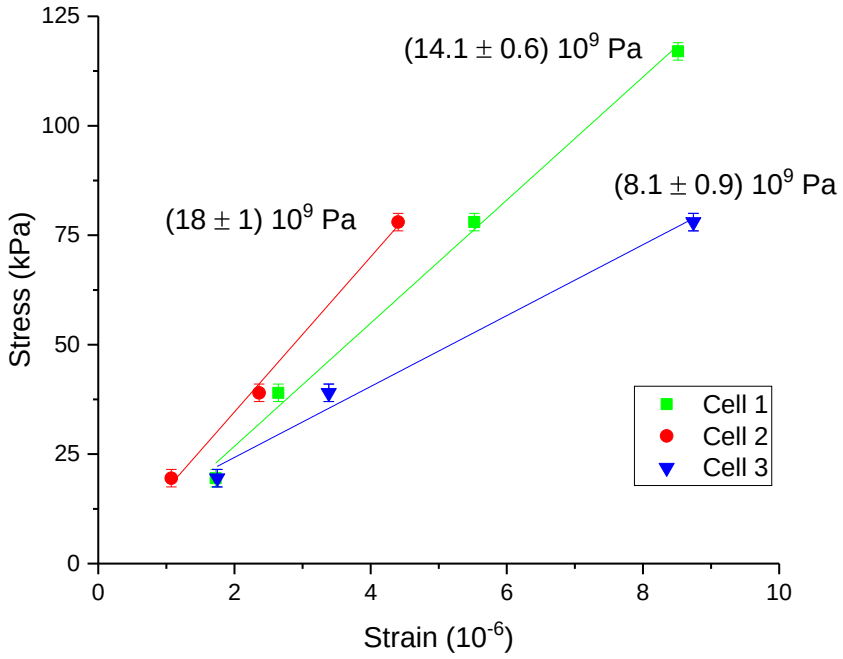

Figure 9 | The stress-strain curve of three different cells. This time only dilute PBS is used. The cells were recorded on different days, and are from different batches of fixed cells. Despite the expected high cell to cell variation, the three cells have generally similar elastic moduli. These are the slopes of the regression, shown beside each curve. The error bars represent the uncertainty of the pressure based on the manufacture's reported error in salinity.

Figure 9 shows the stress-strain curve of multiple cells. Only positive pressures were used to avoid possible discontinuous curves. While different cells do show some variation, the elastic moduli are remarkably similar, and are within the expected range based on vesicle studies[16]. Since membrane tethers are more commonly used to measure whole cells, finding comparing literature values is difficult. Vesicle studies show the elasticity as two magnitudes lower, but it is reasonable to believe that the cytoskeleton contributes that much structures. The cells tested here have also been fixed using formalin, which crosslinks amine groups. This crosslinking would also increase elasticity.

Even though direct comparisons to literature are difficult, these values are reasonable compared to other structures. The results are also linear within the tested range, implying that the algorithm is able to accurate track the edge over this range, and the expansion is happening as expected.

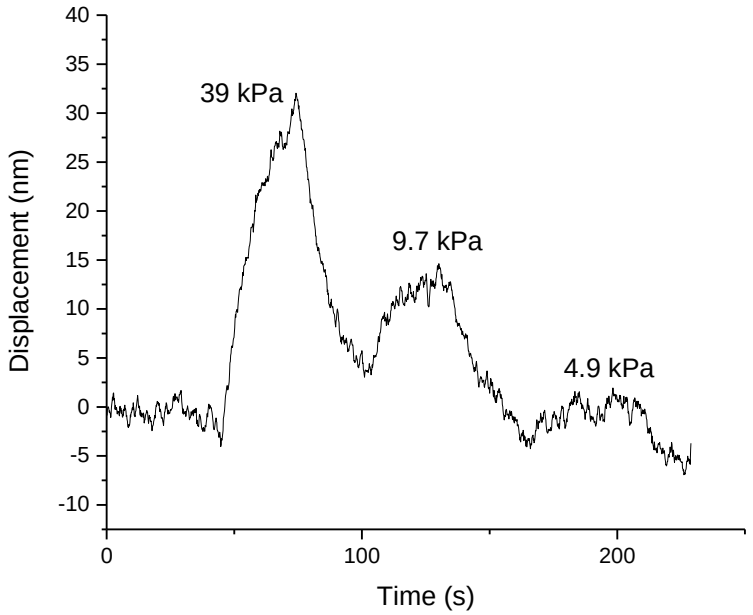

Figure 10 | The expansion from increasing smaller dilutions of PBS. Here one can see that 9.7kPa (adding just 1 part per 40 water to PBS) is the smallest dilution that can be reliably measured. At half that dilution (4.9 kPa or 1 part per 80 water) some change can still be seen, though the magnitude is too small to determine.

Figure 10 shows the limit of detection, with 1/40 dilution being the smallest dilution that can be reliably measured, which is 9.7 kPa of pressure. One part in 80 was also tested, which is 4.9 kPa of osmotic pressure. Some change is seen as a result, but the signal to noise ratio is too small to reliably quantify it. The theoretical limit of detection is 7 kPa, which would give a response three times the noise. Figure 8 shows pressures as

high as 200 kPa were measures, and an upper limited was not determined. This range gives a lot of room to generate a stress-strain curve with many data points.

The potential utility has not been fully explored here, but shows good promise for being a new way to measure the elasticity of plasma membranes. There are a multitude of factors that made this data difficult to compare to literature, but this is because this technology adds a need level of depth to the topic. Comparing it to other technologies and seeing how the elasticity varies with environment can give us a new understanding of how the cytoskeleton and membrane work together. The ease of experiments is also alluring. Typical experiments in this field involve incorporating some kind of tag into the membrane and testing in a complicated setup, using optical tweezers or AFM. Here, a stress-strain curve can be easily generate from one simple experiment using basic equipment and methods. Figures 10 and 8A show that a single curve can be used to get numerous pieces of information all on the same cell.

Chapter 2: Edge Tracking Kinetics

The receptor-ligand driven expansion is poorly understood. This expansion has been tested and explored by previous researchers. Adherent SH-EP α4β2 cells were recorded under 40X phase contrast and found to expand on average 15 nm when introduced to WGA[17]. The same cell line with the cell trapping setup used here expanded 200 nm when WGA was introduced[18]. The large difference between the two methods is likely because of the difference between adherent cells and suspension cells. Adherent cells are attached and their membrane spread taunt over an area. They have much less degree of freedom, which is why loosely attached cells are tested. A comparison of these results is shown in figure 11. Here, the same reaction is tested in a different setup, one that allows simultaneous monitoring with SPR. The cells are cultured on gold chips to allow for SPR monitoring. They are incubated on the gold chips for only 30 minutes, whereas typical adherent cell protocol calls for 12 to 16 hours. This shorter incubation time leaves them only partially adherent, giving better contrast and sharper edges along with slightly larger signals.

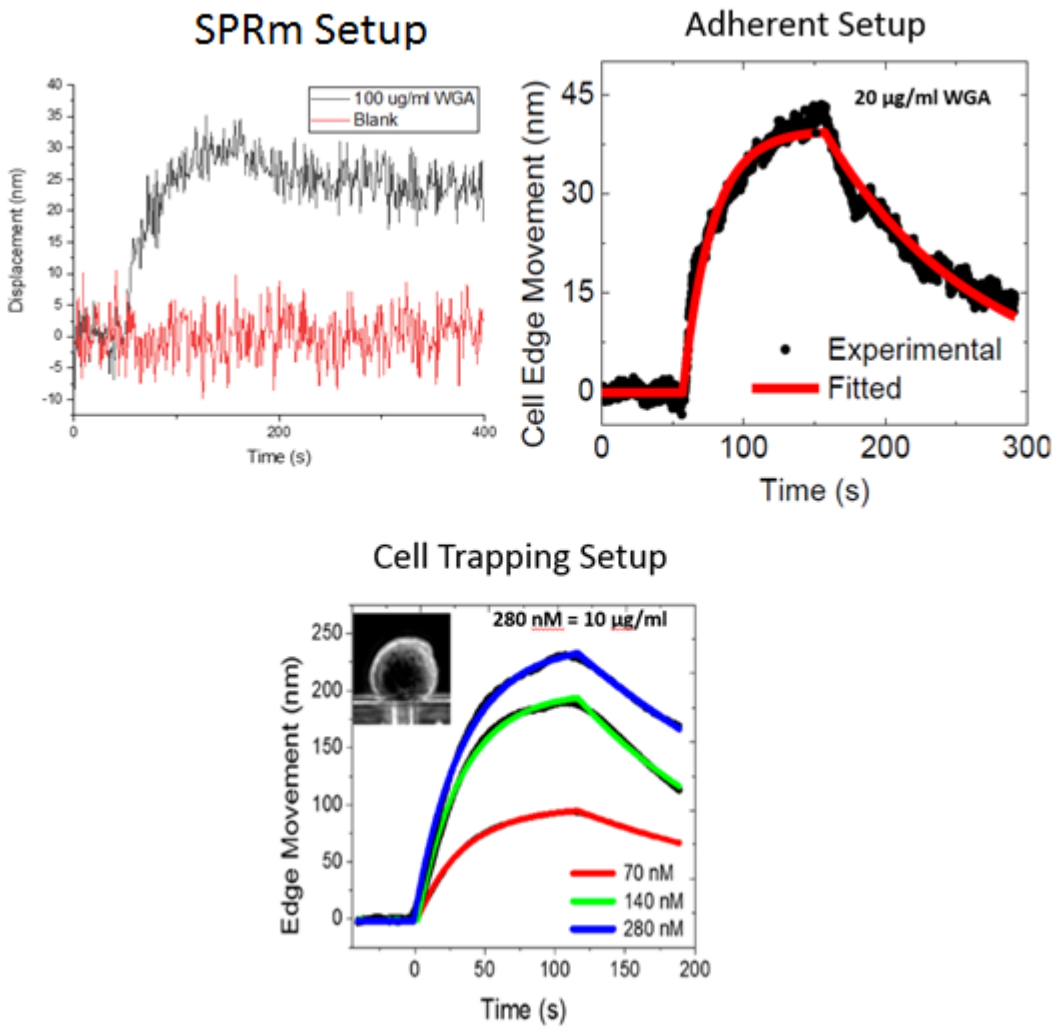

Figure 11 | A comparison of the SPRm setup with the two previous ones. In all figures, there is an initial baseline reading that lasts roughly 30 seconds. Then the association phase lasts from 100 to 150 seconds, when the cell is exposed to WGA. A clear rise in signal is seen during this phase. Finally, the dissociation phase starts, when the cell is no longer exposed to WGA and the bound lectin is left to dissociate and wash away. A gradual decrease is seen during this phase. A, data from the SPRm. The black curve shows the edge movement of a cell when a high concentration of WGA was exposed to it. The red curve shows a blank, when the same injecting process was used but with a vial containing no WGA. B, The adherent setup has a similar signal size with a somewhat better noise level[17]. C, data from the cell trapping setup[18]. The signal is much large than either other setup. Though it is not apparent from the figure, the noise level is also somewhat smaller.

Figure 11 demonstrates that WGA binding can be clearly seen with this new setup. No response is seen in the blank as is expected. Previous works have found the response from the ligand is dependent on available receptors, and no response is seen even with a ligand if there are no receptors on the cell surface[18]. The signal to noise ratio is lower than previous works but this setup gives greater stability, flow control, field of view, and allows for simultaneous SPR measurement, which is impossible in the other setups. The utility of this setup is to measure the SPR signals while also measuring the displacement. This allows us to gauge how accurate the edge tracking method is for gathering kinetic data. However, in order for these comparisons to be useful, the results here need to be established as equivalent to the previous setups. The noise, and therefore error and deviation, may be higher here. However, if the averages are similar, this setup can be trusted to reflect previous works.

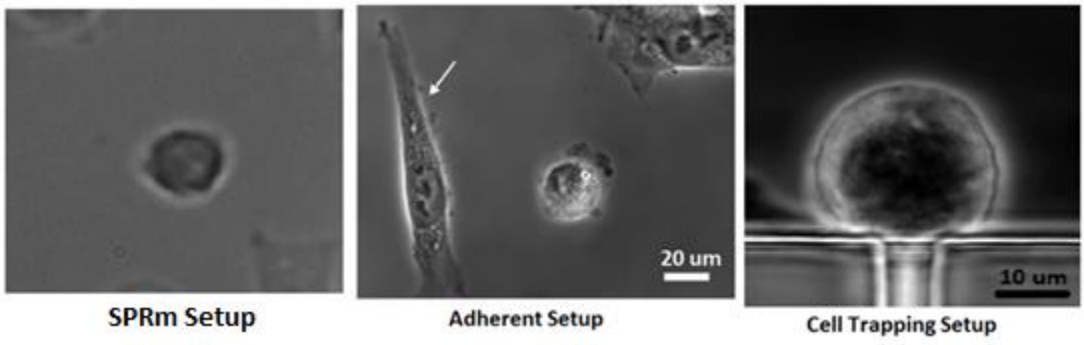

Figure 12 | Images taken from the different setups. The image from the SPRm setup shows a loosely attached cell with a distinct edge. The image from the adherent setup shows a fully attached SH-EP cell with a bright halo typical to phase contrast. Details from inside the cell can also be made out. This image also shows a rounded up cell. Unlike the other setups, where healthy cells are made to be round, this cell is likely round due to it being unhealthy. The trapped cell setup shows a cell, fixed in suspension, trapped against a small pore. This pore had flow going through it, which pulled a cell in suspension towards it. Once pressed against the pore, pressure kept it in place.

Figure 12 shows the images from the different setups. It's clear that the images from the SPRm has lower resolution and less defined edges. This can easily explain the higher noise level. Despite the difference in quality of the images, the noise level only has a modest increase. The noise of the cell trapping setup is the smallest, at 3 nm. The noise in the SPRm setup shown in figure 11 is 10 nm, though optimization has brought it down to 4 nm. This means that despite a less clear image, the noise level doesn't suffer. It's possible that the increased stability of the SPRm lowers noise significantly, and the different setups have different sources of noise.

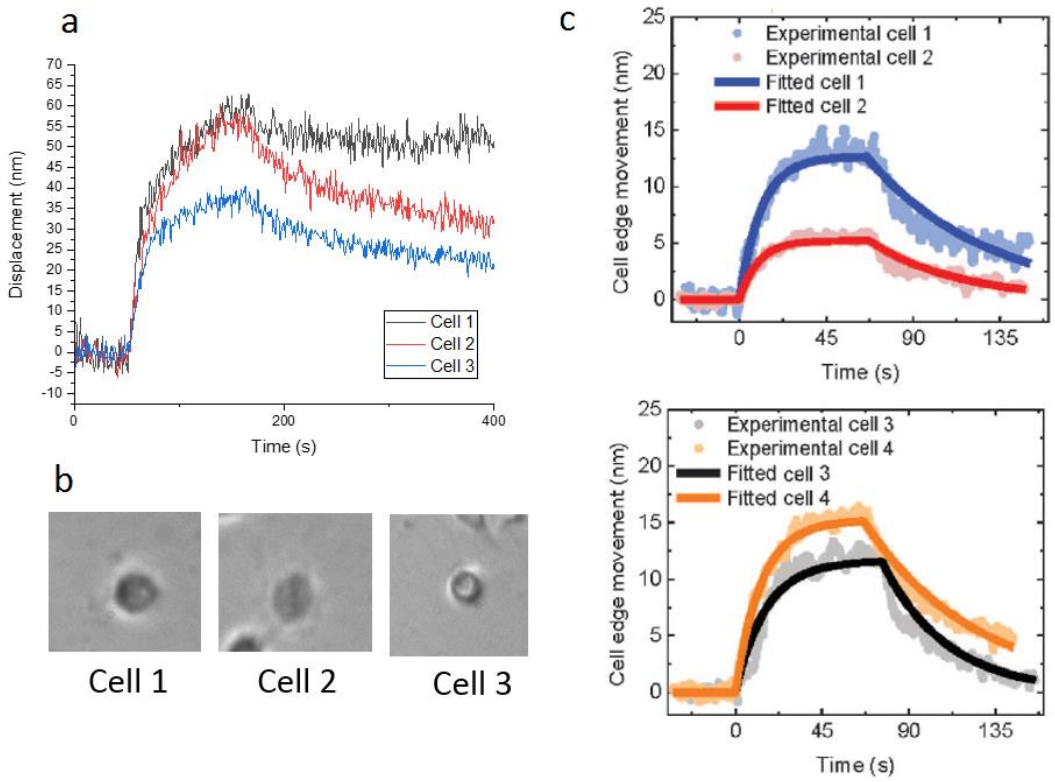

Figure 13 | The cell to cell variability in both rate and extent of binding. In the SPRm setup curves from three different cells were recorded simultaneously. There is cell to cell variation in both the magnitude and rate of the expansion even when recorded simultaneously. The concentration of WGA used was 100 µg/mL. A different reaction is shown in the adherent setup curves, between the small molecule acetylcholine and muscarinic reactions. However a high level of cell to cell variability can still be seen.

WGA binding with glycoproteins is a second order reaction, however under continuous flow it becomes a pseudo first order reaction. Various concentrations of WGA were introduced to the same cells, allowing us to construct a plot of the concentration-dependence of the kinetics constant without cell to cell variability. Previous studies have shown that the binding of WGA to cell surfaces is complex. WGA binds to the sugar N-acetyl-D-glucosamine which is incorporated into many different glycoproteins, each of which can have its own kinetic constant[9,19]. How this sugar is arranged with respect to the rest of the sugars can greatly affect binding[20]. Considering the complexity of the reaction and the heterogeneity of a cell's glycocalyx, it's easy to understand why there is so much cell to cell variability in both extent of binding and also reaction rates, shown in figure 13.

Table 1 | Fit results from various cells compared to previous setup.

SPRm Setup – Edge Tracking			
	k_{on} (M^{-1} s^{-1})	k_{off} (s^{-1})	K_D (nM)
Cell 1	$(6.6 \pm 0.5) \cdot 10^{4}$	$(3.5 \pm 0.3) \cdot 10^{-3}$	53 ± 6
Cell 2	$(11.4 \pm 0.9) \cdot 10^{4}$	$(3 \pm 1) \cdot 10^{-3}$	25 ± 9
Cell 3	$(12.5 \pm 0.5) \cdot 10^{4}$	$(3.0 \pm 0.3) \cdot 10^{-3}$	24 ± 3
Cell 4	$(14.0 \pm 0.5) \cdot 10^{4}$	$(1.9 \pm 0.3) \cdot 10^{-3}$	13.4 ± 2
Mean	$11.1 \cdot 10^{4}$	$2.78 \cdot 10^{-3}$	28.7
SD	$2.8 \cdot 10^{4}$	$0.58 \cdot 10^{-3}$	14.7

Adherent Setup

	k_{on} $(M^{-1}s^{-1})$	k_{off} (s^{-1})	K_D (nM)
Cell 1	$6.92 \pm 0.04 \times 10^{4}$	$1.70 \pm 0.01 \times 10^{-3}$	24.6 ± 0.2
Cell 2	$1.37 \pm 0.02 \times 10^{5}$	$3.34 \pm 0.03 \times 10^{-3}$	24.5 ± 0.3
Cell 3	$8.10 \pm 0.20 \times 10^{4}$	$1.29 \pm 0.02 \times 10^{-3}$	15.9 ± 0.3
Cell 4	$5.70 \pm 0.10 \times 10^{4}$	$0.93 \pm 0.09 \times 10^{-3}$	16.2 ± 0.4
Cell 5	$1.12 \pm 0.02 \times 10^{5}$	$1.45 \pm 0.01 \times 10^{-3}$	12.9 ± 0.2
Cell 6	$1.02 \pm 0.03 \times 10^{5}$	$3.60 \pm 0.03 \times 10^{-3}$	35.5 ± 0.9
Mean	9.30×10^{4}	2.05×10^{-3}	21.6
SD	2.96×10^{4}	1.13×10^{-3}	8.3

Previous works have explored this variation in other setups. The adherent cell setup had a k_{on} standard deviation of 30% of the mean, and the cell trapping setup had a standard deviation of 10% of the mean. This difference in variation could be from higher error in the adherent cell setup, or possibly different status of the cells. The k_{on} standard deviation with the SPRm setup is 28% of the mean. Table 1 shows the fitting results from various cells. The SPRm is in agreement with the adherent cell setup. The mean of the k_{on}

is within one SD each other, with the SD if both data sets being very similar. The means of the k_{off} do vary more, but as still within one SD of each other. Both data sets are small, however considering the means and deviation, it is unlikely that they truly differ by magnitudes. The spread seen in the data is present in the SPR data as well, showing that it is not due to error unique to edge tracking. Table 2 shows similar values from table 1, but using results from SPR instead.

Table 2 | Fit results from various cells found using SPR.

SPRm Setup – SPR			
	k_{on} (M^{-1} s^{-1})	k_{off} (s^{-1})	K_D (nM)
Cell 1	$(6 \pm 1) \cdot 10^{4}$	$(4.6 \pm 0.2) \cdot 10^{-3}$	77 ± 13
Cell 2	$(10 \pm 3) \cdot 10^{4}$	$(5.1 \pm 0.2) \cdot 10^{-3}$	51 ± 15
Cell 3	$(10 \pm 3) \cdot 10^{4}$	$(6.2 \pm 0.3) \cdot 10^{-3}$	62 ± 19
Cell 4	$(10 \pm 1) \cdot 10^{4}$	$(7.3 \pm 0.2) \cdot 10^{-3}$	73 ± 8
Cell 5	$(10 \pm 1) \cdot 10^{4}$	$(6.7 \pm 0.2) \cdot 10^{-3}$	67 ± 7
Cell 6	$(11 \pm 1) \cdot 10^{4}$	$(4.4 \pm 0.2) \cdot 10^{-3}$	40 ± 4
Mean	$8.36 \cdot 10^{4}$	$2.78 \cdot 10^{-3}$	60
SD	$2.26 \cdot 10^{4}$	$0.58 \cdot 10^{-3}$	12.7

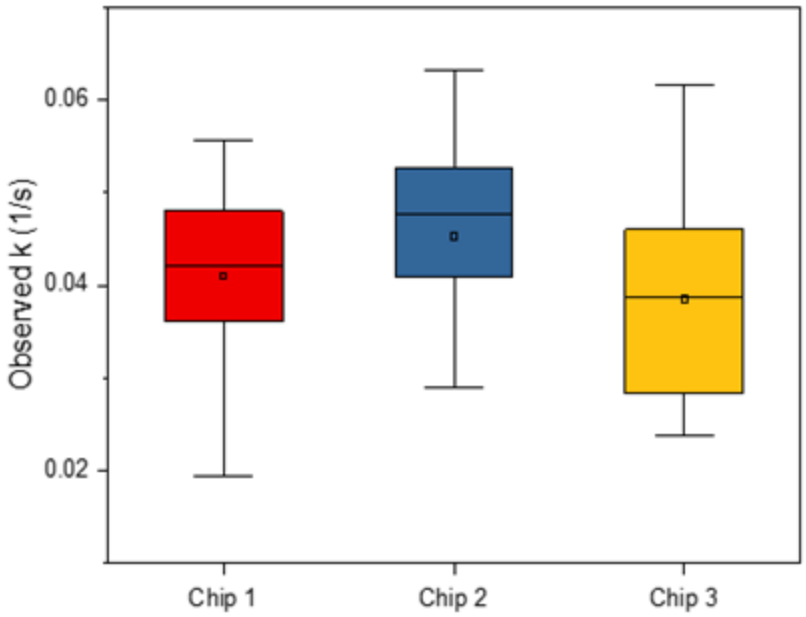

Figure 14 | A box and whisker plot of the observed kinetics constant from 3 different chips. Each chip has at least a dozen cells, and all cells were exposed to 100 µg/mL WGA for this figure. Experiments were performed on different days. This figure shows that while there are some chip to chip variations, it is much smaller than cell to cell variation and likely can be entirely explained by it. The accompanying table provides the statistics of the box and whisker plot.

Table 3 | The averages and standard deviations from figure 14.

	Chip 1	Chip 2	Chip 3
N	20	13	13
Average	$4.10 \cdot 10^{-2}\ s^{-1}$	$4.53 \cdot 10^{-2}\ s^{-1}$	$3.85 \cdot 10^{-2}\ s^{-1}$
SD	$0.96 \cdot 10^{-2}\ s^{-1}$	$0.99 \cdot 10^{-2}\ s^{-1}$	$1.09 \cdot 10^{-2}\ s^{-1}$

Figure 14 shows the variation seen within the SPRm setup, between and within chips. There is significant variation with the kinetics, and previous data has already shown. This is true for cells recorded at the same time as well, and does not vary with location on chip. Thus further supports the idea that there is inherent and genuine cell to

cell variability. The box and whisker plot in figure 14 shows a more comprehensive view of the variation within a chip and between chips. Each chip has at least a dozen cells, and the different chips were tested on different days. The chip to chip variation seems to be smaller than the cell to cell variation. In particularly, all the standard deviations are similar, and none of the means different by more than 1 SD. This implies that there is high cell to cell variation. This is inherent to the cells but the method itself appears consistent chip to chip based on this preliminary data.

All these results clearly show that the SPRm produces similar results as previous works, in particular the adherent cell setup. Significant variation exists, but this is probably inherent to variation of the cell membrane. Some error exists within the method, in particular the noise when recording displacement. However this noise is much smaller than expected for the resolution and can be further minimized to be only slightly higher than the adherent setup. Regardless of the source of noise, neither that mean nor the spread of fitting results differs greatly from previous setups. The SPRm can then be trusted to represent the results of other methods.

Chapter 3: SPR comparisons

The novelty of the setup used is that it allows for dual monitoring with SPR and bright field. Previous setups reported kinetic constants that agree with literature. However, due to the high cell to cell variability it was hard to gauge just how accurate the values were. On top of that, differences in platforms and research groups also introduce some discrepancies as well. That is why simultaneous measurements with SPR are so useful.

They remove both of these sources of error by testing the same cells on the same platform.

Figure 15 shows the edge tracking response overlaid with the SPR response.

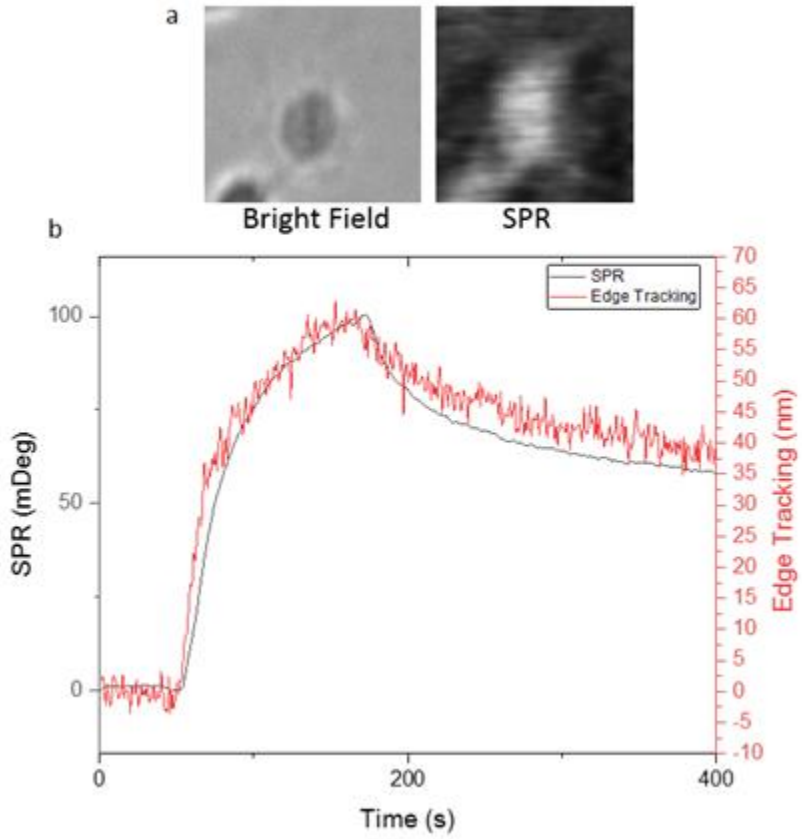

Figure 15 | Comparison of both images and curves from bright field and SPR. a, images of the same cell at the same time taken with bright field (left) and SPR (right). b, the curves from the two videos overlaid on top of each other. It can be seen that they largely agree, though the edge tracking is much noisier. It should be noted that in optimized setups for edge tracking, the noise is comparable to SPR for this reaction[18]. With other reactions involving small molecule, the edge tracking algorithm can detect binding that the SPR signals are too small to detect.

Figure 15 shows the edge tracking response overlaid with the SPR response. The two curves appear very similar, although the edge tracking curve has higher noise. The conversion factor between edge displacement and SPR signal is of some interest. The

SPR signal is well understand and meaning can be derived from its magnitude. Because edge displacement is less well studied, it's unclear what meaning can be derived from the extent of binding. It can then be helpful to relate nanometers of displacement to the SPR response. When searching for the best agreement between the association phases the average conversation factor was 3.13 mDeg per nm, and the standard deviation was 0.77 mDeg per nm. This factor does not seem to correlate with anything obvious, though further investigation would be needed for more confidence. It can be tentatively used to estimate WGA bound based on nanometers of displacement.

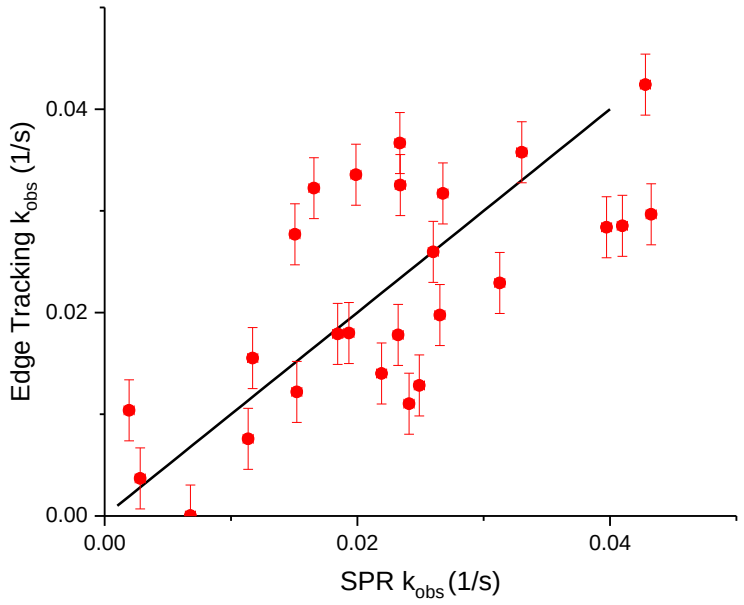

Figure 16 | Plot of the observed kinetics constant from the edge tracking algorithm and the SPR data from simultaneously measured cells. Each dot represents a single cell that has both SPR data and edge tracking data for the same binding events. Though not tightly correlated, the relationship is close to the expected one-to-one ratio. The solid, black line represents the expected one to one ratio.

The observed kinetic rates found from edge tracking were plotted against the rates found from SPR to show how well they agree. The expected plot has a one to one ratio

for the slope, and no intercept. Figure 16 shows both the expected and actual data. When a linear regression with a set intercept of zero is done on the data, the slope is 0.97, very close to the ideal 1. This means that the binding kinetics from edge tracking do represent the true binding kinetics. Despite the good agreement, the correlation appears loose.

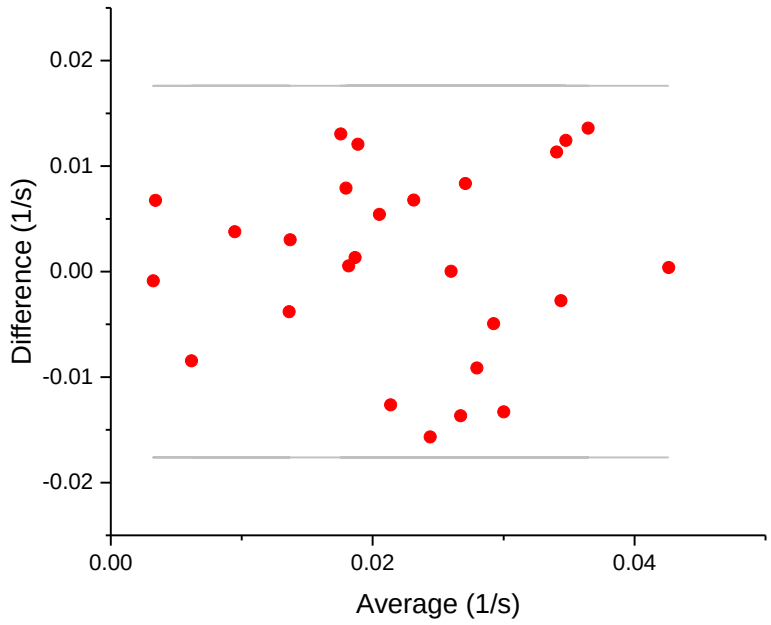

Figure 17 | The Bland-Altman plot showing the discrepancies between SPR and the edge tracking algorithm with more detail. The standard deviation of the difference between the two methods is 0.009 s^{-1}. The gray lines mark plus and minus two times the standard deviation, ± 0.018 s^{-1}.

Bland Altman plots, like shown in figure 17, are more useful for giving greater detail of the errors between the two methods. There are two key points to note from figure 17, the first being that the difference does not increase with the kinetics constant, at least not within the tested range. This simplifies comparison, and implies that the method is valid within the tested range. Secondly, the standard deviation of the difference between the methods is 0.009 s^{-1}, with all the data points being within ± 0.018 s^{-1}. This difference in

the methods is about the same as the standard deviation between cells from the same run, shown in figure 9. The range of the different cells shown in figure 9 is larger than the range of differences, about 0.037 s^{-1}. Cell to cell variation is more prominent than the difference between the methods. If working with many cells and trying to find an average kinetic constant, the error from this method would be secondary to the variation between cells. It's also fair to speculate that this difference between methods would be smaller with the lower noise of the cell trapping setup.

The kinetics results from the edge tracking agree with the SPR results. As with any two methods, there are discrepancies. However, edge tracking is neither consistently higher nor lower, and on average is the same. The error that does exist is symmetrical. This gives the ideal one to one ratio seen in figure 16. The difference between the two methods is consistent, and doesn't vary with the kinetics constant. It's also similar to the cell to cell variation, with the spread being even smaller. Edge tracking as a means of measuring binding kinetics does give results that reflect actual kinetics constants and the error is less than the error introduced from cell to cell variation.

Chapter 4: Noise Analysis

In order to help gauge the sources of error, polystyrene microbeads were used to study noise. These beads are half the size of the cells but are rigid and solid. By examining them, the error inherent to the system can be examined without the movement inherent to the micromovement of cells. This can help get a hold of the true error, excluding cell to cell variation.

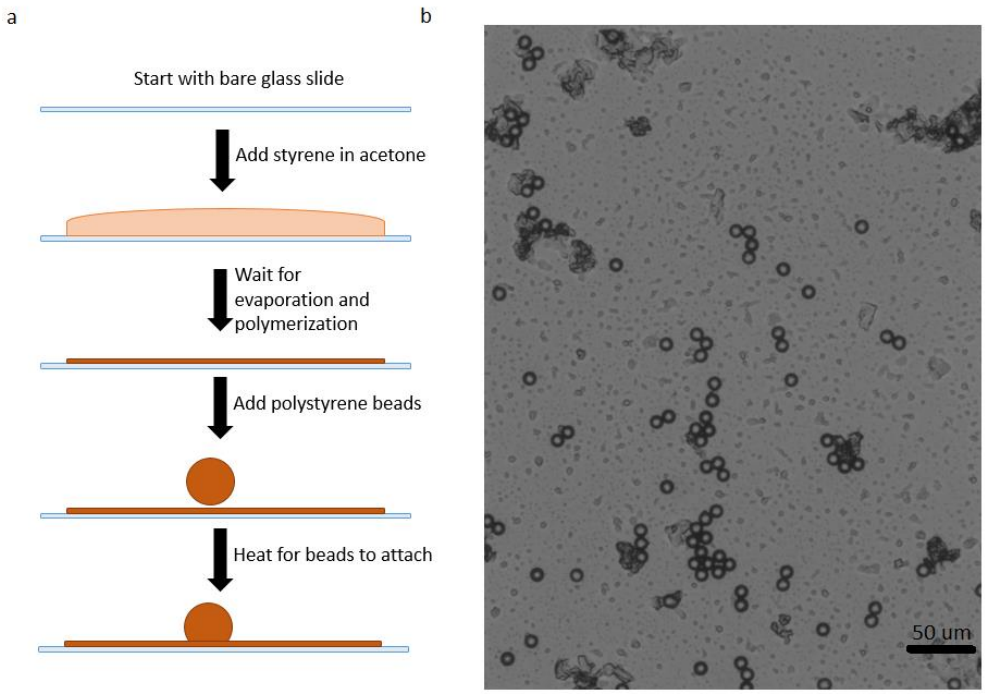

Figure 18 | An image of the polystyrene beads under 40X, phase contrast microscopy and how the chips are made. a, the protocol used to attach beads. A glass slide is coated with a solution of styrene in acetone. As the acetone evaporates, the styrene polymerizes onto the surface, creating a thin layer of polystyrene. Polystyrene beads are then added and the chip is heated to 60° C overnight. This causes the beads to soften and attach to the polystyrene on the surface. b, an image of the beads. Some of the beads are clumped together, which were not used for noise analysis. Only lone-stranding beads were used, though the edge tracking algorithm could treat a clump of beads or cells as a single object. The lighter, small objects are due to uneven coating of the polystyrene modification. This can be reduced by using a less concentrated polystyrene solution to modify the chips. However, because the imperfections were stationary they did not affect the edge tracking algorithm.

For this setup a 10X objective was used, similar magnification as with the SPRm. A glass slide was modified with a thin layer of polystyrene and 10 μm beads were evaporated onto the chip. The chips were heated to 60° C overnight before use. Water was added to the chips and they were recorded under various light levels. Figure 18 shows an image from these experiments. The beads are easy to see, with dark edges and a

brighter inside. Many beads were clumped together. The edge tracking algorithm can track clumps as one object, but to avoid possible complications only single beads were monitored. Lighter gray specks and darker, larger objects are seen scattered around. These are likely larger segments of polystyrene from the surface modification. The larger objects were avoided, and the small patches did not contribute to noise because of how stationary they were. These patches could be minimized with more optimization of the chip modification protocol.

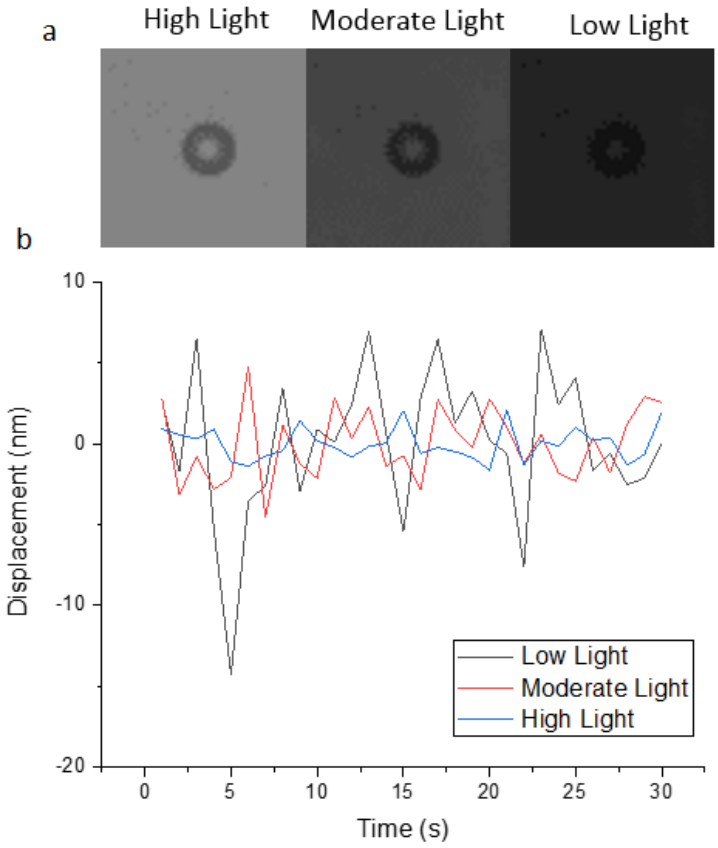

Figure 19 | Figure showing the impact of light levels on noise. a, Images of the same bead at three different light levels, ranging from high light levels (left) to low light levels (right). b, Brief, 30 second recordings of the bead under the different light levels. In this instance, the light levels were not quantified. They were caused by adjusting the brightness of the microscope's light source. A significant reduction of the noise can be seen with increasing light levels.

Single beads were chosen throughout the field of view. These beads were monitored as the light level was adjusted. Figure 19A shows a bead in three different light levels, with the high light level being just below saturation and the low light level being barely visible. Figure 19B shows 30 seconds recordings of the bead in these three different light levels. There is a large decrease in noise from the low light to the high light levels. This is what is expected when shot noise dominates, which it seems to do in lower light levels.

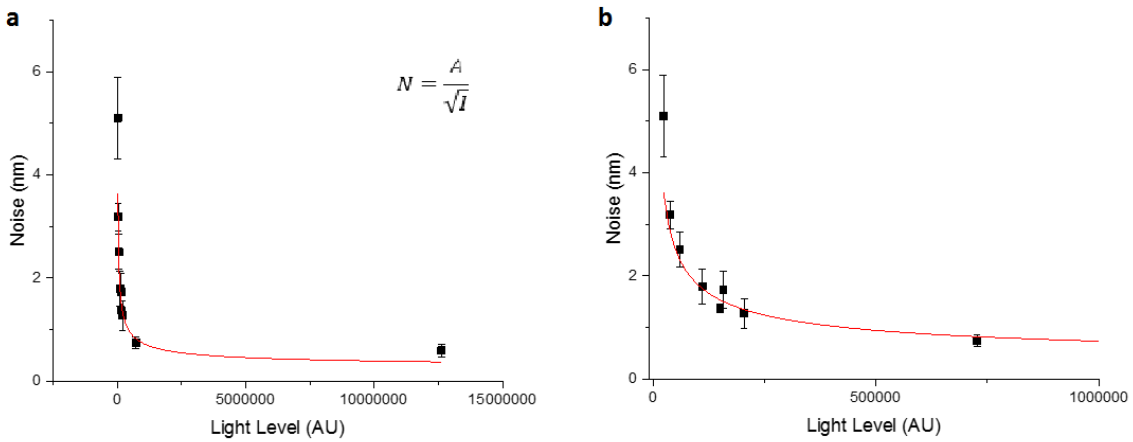

Figure 20 | Plots showing graphically how noise decreases with light. a, the noise level from the recordings as shown in figure 19b, defined as the standard deviation of the baseline. The noise level of five beads were averaged together for each data point. The error bars are the standard deviation of the noise levels. The light level is an arbitrary unit proportional to the number of photons captured a second. The red line shows a fit using an inverse square root model, the relationship between shot noise and light level[21]. b, a magnified section from part a that excludes the highest light level. This shows the decrease with light level.

Five beads were recorded in multiple different light levels, and the standard deviation of their baseline was measured and used as the noise level. The five different

beads were averaged to get the data points shown in figure 20. Because shot noise was expected to dominate for the light levels shown in figure 20B, the model for the curve fitting was the relationship shot noise has with light level, an inverse square root relationship. This model fits the data at the lower light levels well, implying that shot noise is in fact predominant at those levels. However, in figure 20A, the data point in the highest light level is significantly above the model fit. This implies at those light levels, shot noise ceases to dominate and has been minimized. Since most experiments were run at high light levels, the shot noise was likely a minimal contributor to the noise level.

Conclusions and Future Directions

This is a continuation of other works on the power of edge tracking. The algorithm allows for a way to quantify small changes with modest lab equipment. This is shown to be a powerful way to measure binding kinetics of both large and small molecule binding, and deformation from osmotic pressures. Because of how general edge deformation is, it's possible this algorithm has utility with other topics as well, although binding kinetics is one if its most promising uses. Binding kinetics are traditionally difficult to get, and the results are questionable depending on the methods used. This technology gives a label free, continuous, and extraction free way to measure kinetics. Though only large molecules were used here, that is simply because SPR can only detect large molecules. Previous works have found it can work with small molecules as well[17,18]. A lot of research has been done into this use, and with this work it becomes clearer that these values are valid and accurate. Future works can focus on finding a high throughput way to measure cells. This would likely involve designed a microfluidics device to

contain cells and introduce ligands. This would be very useful, since usually many potential drug candidates are tested with the hopes of just one going to market.

Though binding kinetics was the most explored topic, there are other utilities. Any situation where the cell membrane is expected to deform, even slightly, could have this technology used. In this work, cell deformation with osmotic pressure was explored. This work only covered the topic briefly, enough to show that it's possible to get reasonable stress-strain curves with both positive and negative pressures and that the range of potential pressures is wide. The principles have been shown here, but a lot more work can be done. Finding the relationship between the elasticity and commonly measured tension can be explored to make this work more relatable to other works. Other directions can be to explore the elasticity of different cell types, including diseased cells, fixation methods and levels, and if various drugs affect elasticity. Despite this topic being generally overlooked, there are many applications.

Works Cited

1 Overington, J. P., Al-Lazikani, B. & Hopkins, A. L. How many drug targets are there? *Nat Rev Drug Discov* **5**, 993-996 (2006).

2 Alberts, B. *et al.* Molecular Biology of the Cell (Garland, New York, 2002). *Google Scholar*.

3 Bogaert, M. Clinical pharmacokinetics of glyceryl trinitrate following the use of systemic and topical preparations. *Clinical pharmacokinetics* **12**, 1-11 (1987).

4 Tenorio, A. T., Boom, R. M. & van der Goot, A. J. Understanding leaf membrane protein extraction to develop a food-grade process. *Food chemistry* **217**, 234-243 (2017).

5 Boussambe, G. N. M. *et al.* (Elsevier, 2018).

6 Jørgensen, I. L., Kemmer, G. C. & Pomorski, T. G. Membrane protein reconstitution into giant unilamellar vesicles: a review on current techniques. *European Biophysics Journal* **46**, 103-119 (2017).

7 Bordbar, A. *et al.* Personalized whole-cell kinetic models of metabolism for discovery in genomics and pharmacodynamics. *Cell systems* **1**, 283-292 (2015).

8 Lundbæk, J. A., Collingwood, S. A., Ingólfsson, H. I., Kapoor, R. & Andersen, O. S. Lipid bilayer regulation of membrane protein function: gramicidin channels as molecular force probes. *Journal of The Royal Society Interface* **7**, 373-395, doi:10.1098/rsif.2009.0443 (2010).

9 Boldt, D. H. Interaction of wheat germ agglutinin with human peripheral blood mononuclear cells. Binding kinetics and flow microfluorometric analysis. *Molecular immunology* **17**, 47-55 (1980).

10 Roylance, D. Stress-strain curves. *Massachusetts Institute of Technology study, Cambridge* (2001).

11 Bianchi, L. Mechanotransduction: touch and feel at the molecular level as modeled in Caenorhabditis elegans. *Molecular neurobiology* **36**, 254-271 (2007).

12 Lieber, A. D., Yehudai-Resheff, S., Barnhart, E. L., Theriot, J. A. & Keren, K. Membrane tension in rapidly moving cells is determined by cytoskeletal forces. *Current Biology* **23**, 1409-1417 (2013).

13 Simunovic, M. & Voth, G. A. Membrane tension controls the assembly of curvature-generating proteins. *Nature communications* **6** (2015).

14 Pontes, B., Monzo, P. & Gauthier, N. C. in *Seminars in Cell & Developmental Biology*. (Elsevier).

15 Dai, J., Sheetz, M. P., Wan, X. & Morris, C. E. Membrane tension in swelling and shrinking molluscan neurons. *Journal of Neuroscience* **18**, 6681-6692 (1998).

16 Hallett, F. R., Marsh, J., Nickel, B. G. & Wood, J. M. Mechanical properties of vesicles. II. A model for osmotic swelling and lysis. *Biophysical journal* **64**, 435-442 (1993).

17 Guan, Y. *et al.* Kinetics of small molecule interactions with membrane proteins in single cells measured with mechanical amplification. *Science Advances* **1**, doi:10.1126/sciadv.1500633 (2015).

18 Zhang, F. *et al.* Label-Free Quantification of Small-Molecule Binding to Membrane Proteins on Single Cells by Tracking Nanometer-Scale Cellular Membrane Deformation. *ACS nano* **12**, 2056-2064 (2018).

19 Monsigny, M., Roche, A.-C., Sene, C., Maget-Dana, R. & Delmotte, F. Sugar-Lectin Interactions: How Does Wheat-Germ Agglutinin Bind Sialoglycoconjugates? *European Journal of Biochemistry* **104**, 147-153, doi:10.1111/j.1432-1033.1980.tb04410.x (1980).

20 Bhavanandan, V. P. & Katlic, A. W. The interaction of wheat germ agglutinin with sialoglycoproteins. The role of sialic acid. *Journal of Biological Chemistry* **254**, 4000-4008 (1979).

21 Jacubowiez, L., Roch, J.-F., Poizat, J.-P. & Grangier, P. in *PROCEEDINGS-SPIE THE INTERNATIONAL SOCIETY FOR OPTICAL ENGINEERING*. 166-179 (SPIE INTERNATIONAL SOCIETY FOR OPTICAL).